

Supporting Information

Synthesis of Naphthalenediimide-Based Cyclophanes for Controlling Anion-Arene Interactions

Yongjun Li,*^a Yingjie Zhao,^a Runsheng Jiang,^a Huibiao Liu^a and Yuliang Li*^a

^a Beijing National Laboratory for Molecular Sciences (BNLMS), CAS Key Laboratory of Organic Solids, Institute of Chemistry, Chinese Academy of Sciences, Beijing 100190, P.R. China.
Fax: (+) 86-10-82616576; Tel: (+) 86-10-62587552;
E-mail: liyj@iccas.ac.cn, ylli@iccas.ac.cn

Table of contents

S1. Experimental	S2
S2 ^1H NMR and ^{13}C NMR spectra	S3
S3. VT ^1H NMR studies of nabp	S7
S4. Cyclic Voltammetry (CV)	S8
S5. Binding Studies	S8
S6. Anion exchange experiments	S17
S7. X-ray diffraction	S20

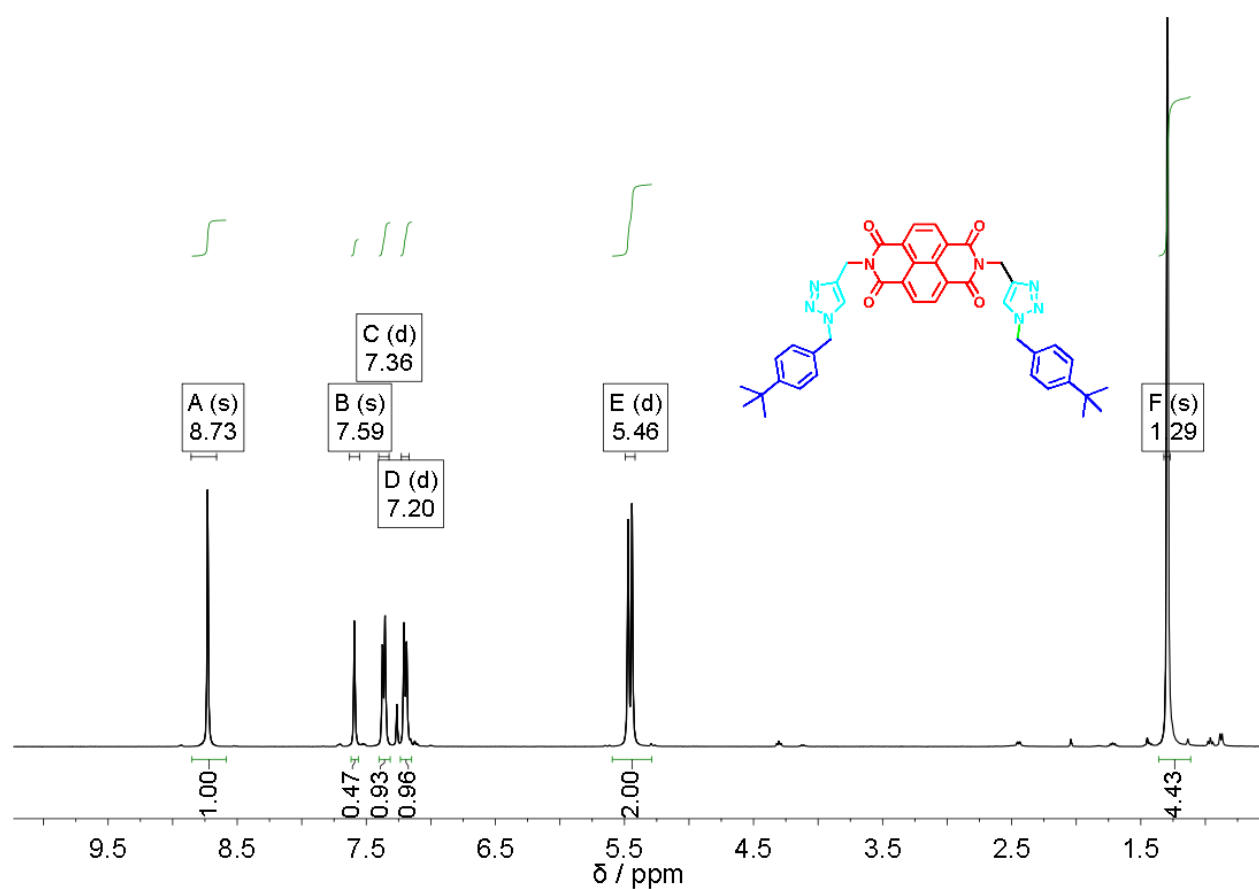
S1. Experimental

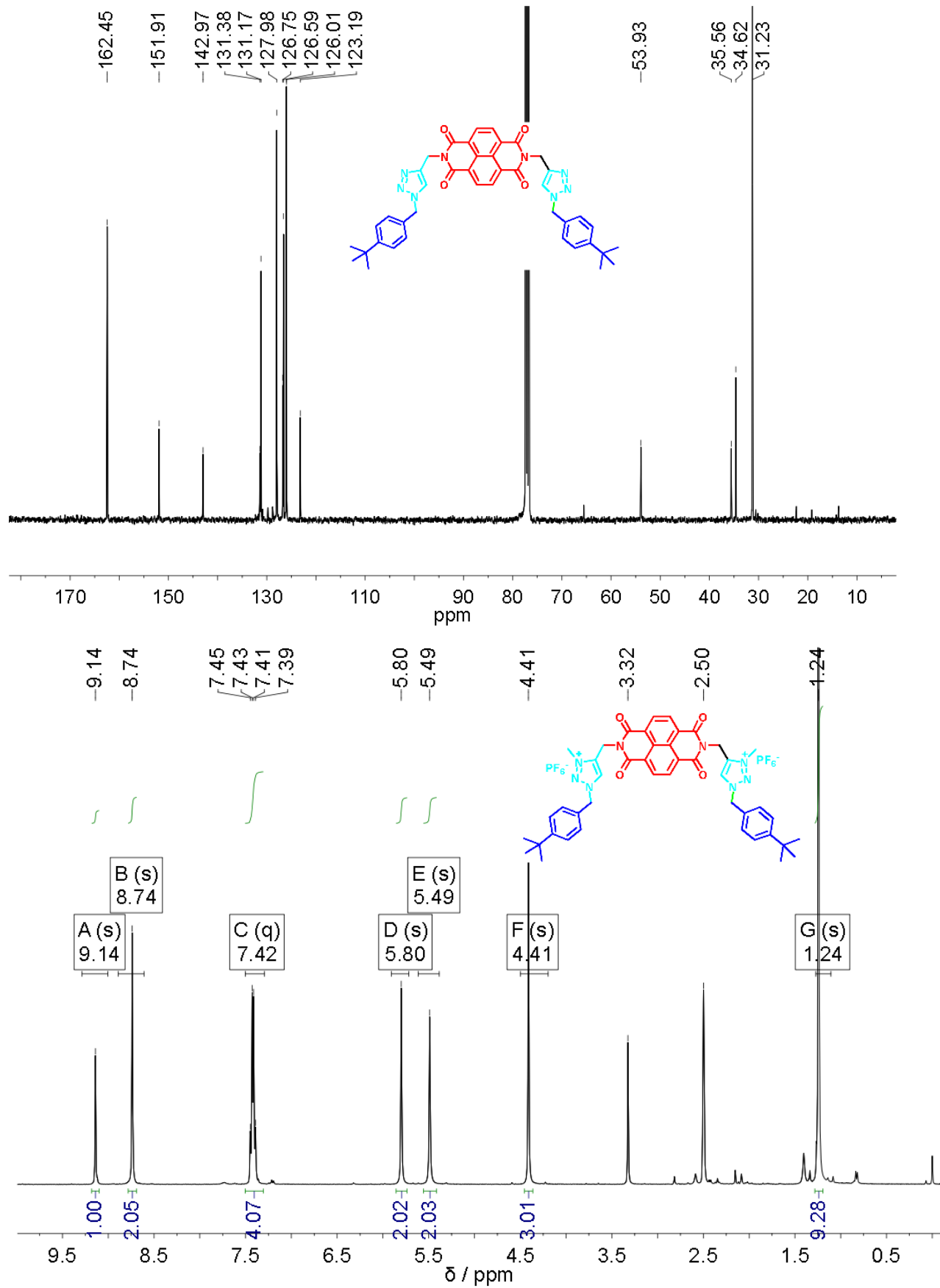
General

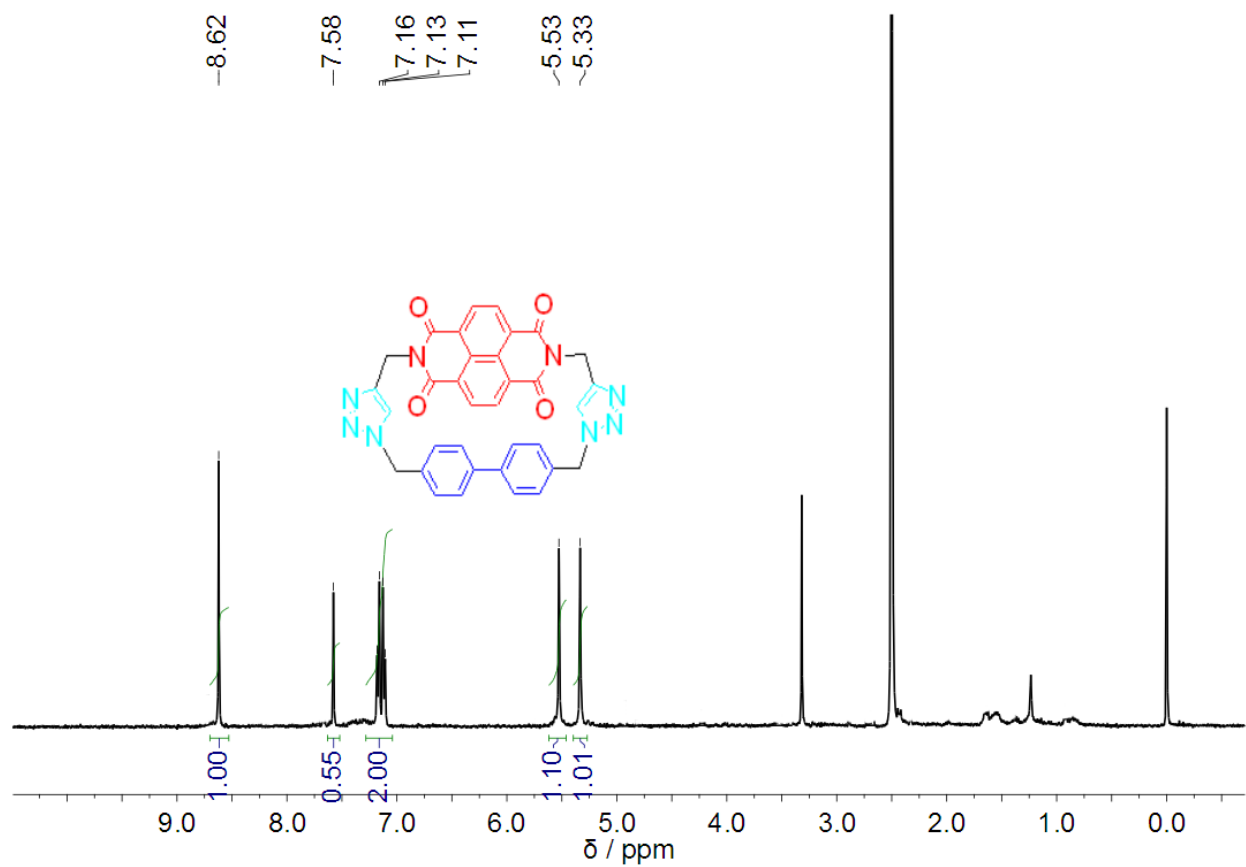
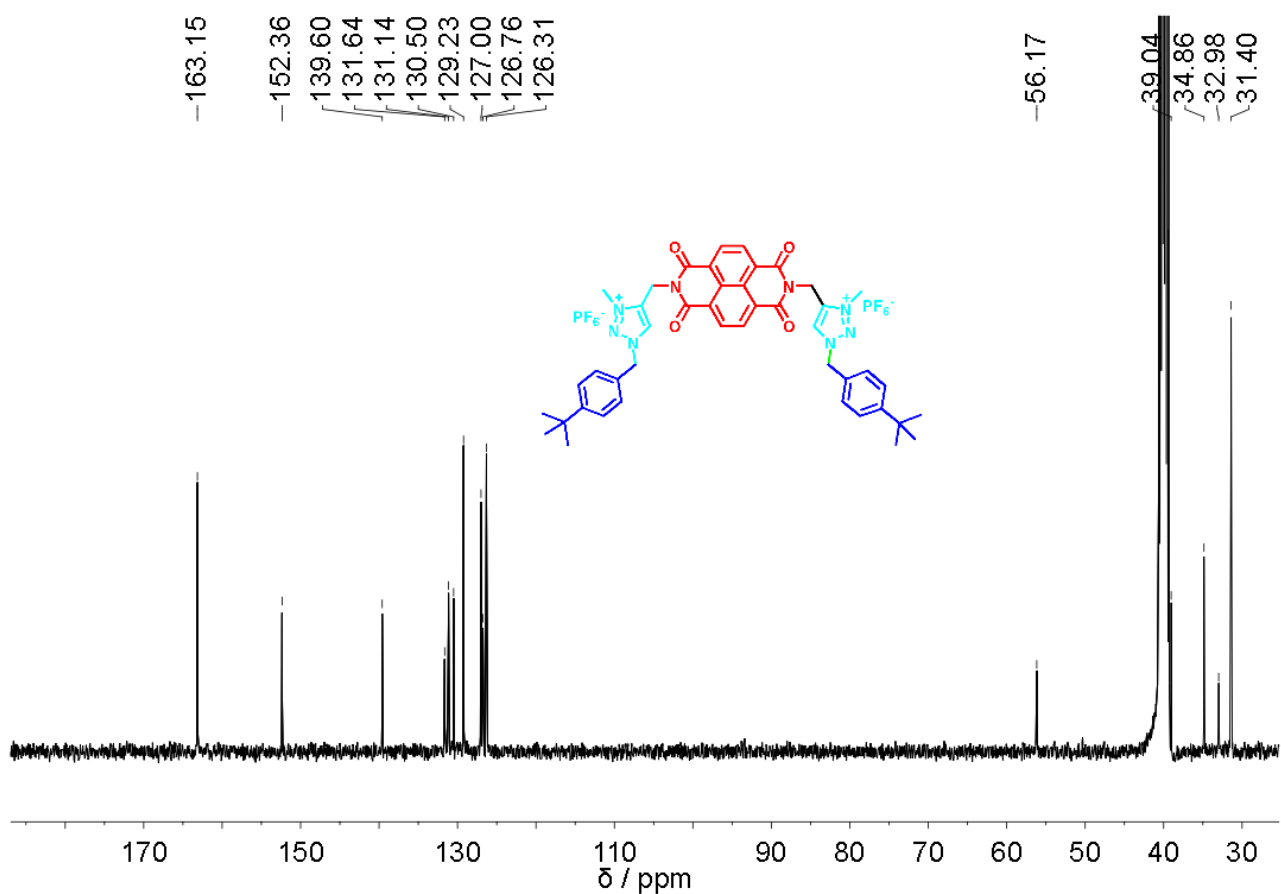
All reagents were obtained from commercial suppliers and used as received unless otherwise noted. Column chromatography was performed on silica gel (160 - 200 mesh), and thin-layer chromatography (TLC) was performed on precoated silica gel plates and observed under UV light. Nuclear magnetic resonance (NMR) spectra were recorded on Bruker Avance DPS-400 and Bruker Avance DPS-600 spectrometers at room temperature (298 K). Chemical shifts were referenced to the residual solvent peaks. Matrix-assisted laser desorption/ionization reflectron time-of-flight (MALDI-TOF) mass spectrometry were performed on a Bruker Biflex III mass spectrometer. Electronic absorption spectra were measured on a JASCO V-579 spectrophotometer. Fluorescence excitation and emission spectra were recorded using a Hitachi F-4500. All single crystal X-ray diffraction data were collected on a Rigaku Saturn X-ray diffractometer with graphite-monochromator Mo-K α radiation ($\lambda = 0.71073 \text{ \AA}$) at 173 K. Intensities were corrected for absorption effects using the multi-scan technique SADABS (Siemens Area Detector Absorption Corrections). The structures were solved by direct methods and refined by a full matrix least squares technique based on F2 using SHELXL 97 program (Sheldrick, 1997). The extended packing plots and data from crystal packing were obtained using the software Mercury 1.4.1.

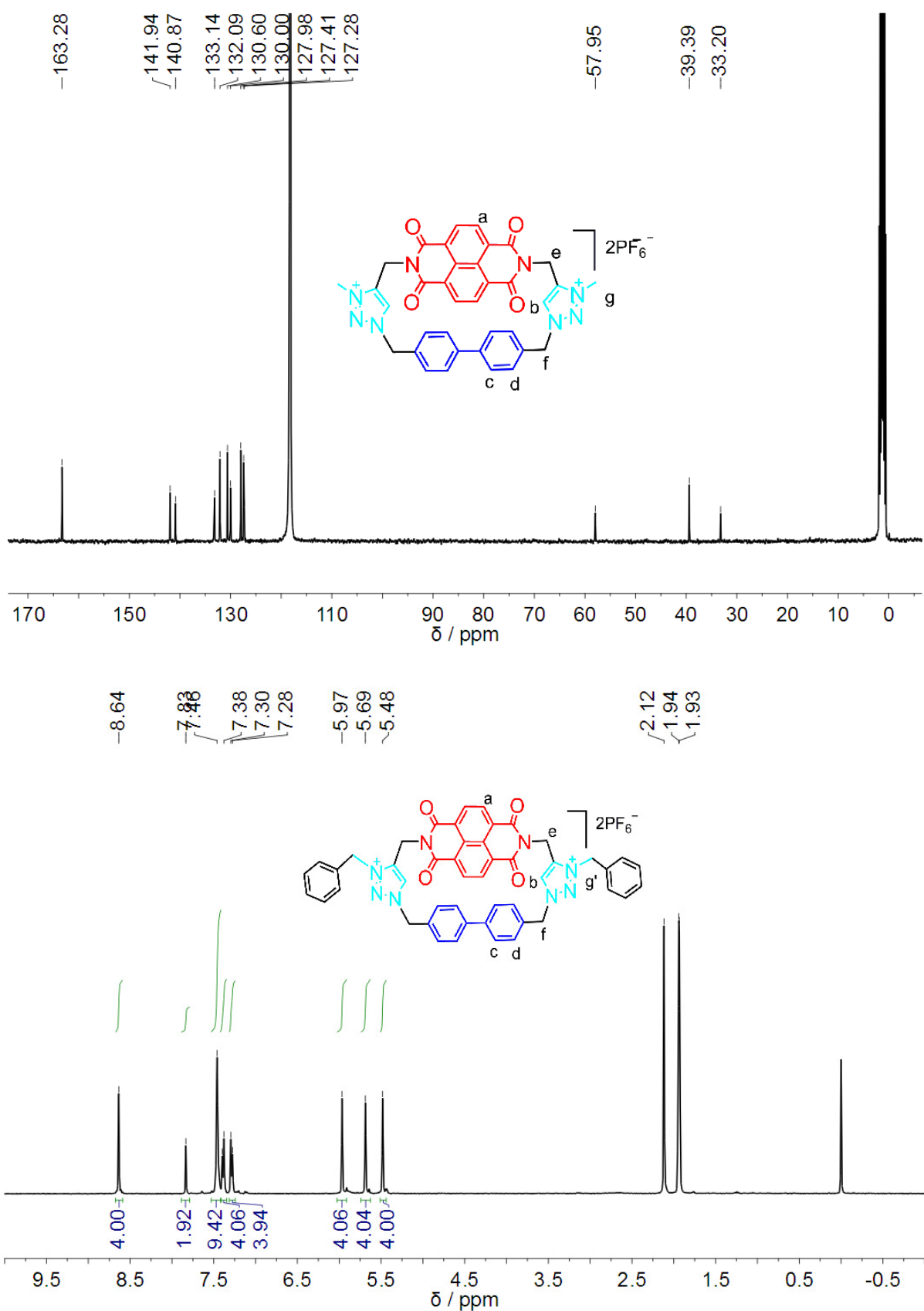
Safety Comment: Sodium azide is very toxic, personal protection precautions should be taken. As low molecular weight organic azides are potential explosives, care must be taken during their handling. Generally, when the total number of carbon (N_C) plus oxygen (N_O) atoms is less than the total numbers of nitrogen atoms (N_N) by a ratio of three, i.e., $(N_C + N_O) / N_N < 3$, the compound is considered as an explosive hazard. In those instances, the compound was prepared prior to use and used immediately. A standard PVC blast shield was used when necessary.

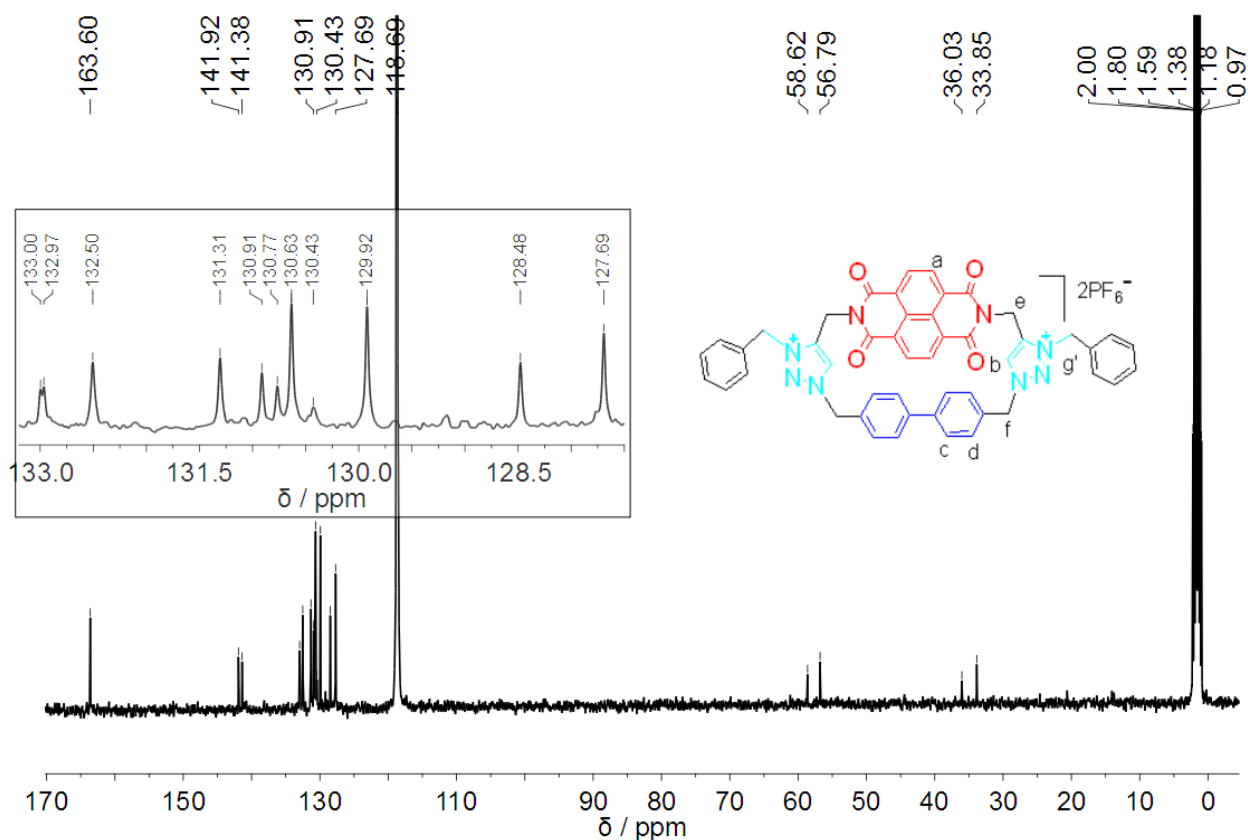
S2 ^1H NMR and ^{13}C NMR spectra





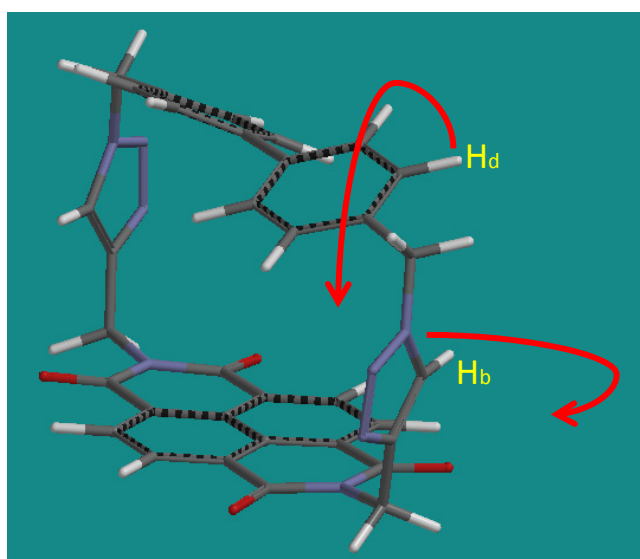






S3. VT ^1H NMR studies of nabp.

NMR spectra of **nabp** at room temperature indicate that the biphenylene moiety rotates rapidly on the NMR time scale. However, upon decreasing the temperature from 298 to 183 K the dynamic processes are slowed, resulting in separation of the signals and the coalescence temperature is at about 298 K. At the same time, the triazole proton H_b and the biphenylene proton H_d (close to triazole) shifted down-field with the decreasing of the temperature, which is consistent with the shielding effect between triazole and biphenylene groups when the movement of triazole and biphenylene groups were slowed.



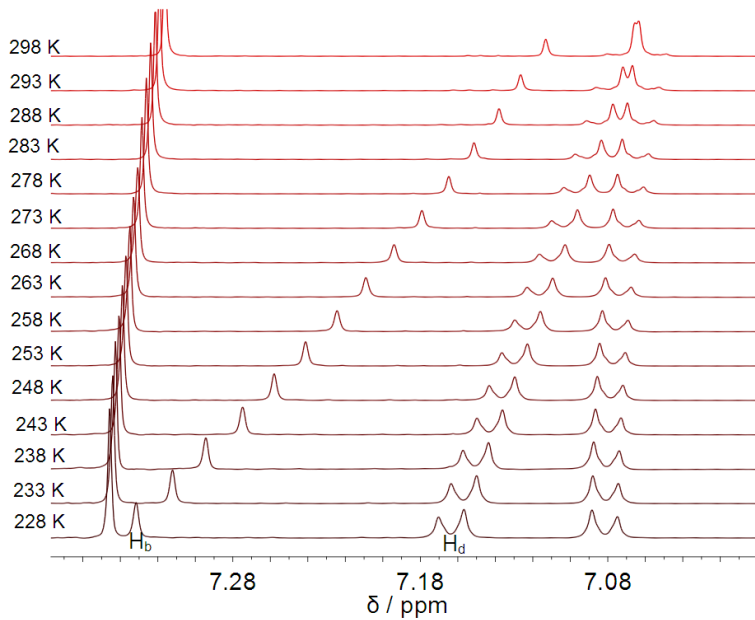


Figure S1. Temperature-dependent NMR signals of the naphthalene ring (600 MHz in CDCl_3) of compound **nabp**.

S4. Cyclic Voltammetry (CV)

CV was carried out using a computer-controlled potentiostat (CHI 600C) and a standard three electrode arrangement that consisted of both platinum working and auxiliary electrodes and a saturated calomel reference electrode. All electrochemical measurements were carried out in N_2 -purged dry DMF with 0.1 M TBAPF₆ as the supporting electrolyte. The scan rate for the measurements was typically 50–200 mV/s. CV studies of the molecules **nabp** and **nabp-Me₂²⁺•2PF₆⁻** (0.1 mM) has been performed in degassed DMF under Ar atmosphere. All the experiments were carried out in dry and degassed DMF at 0.1 mM concentration of **nabp-Me₂²⁺•2PF₆⁻** and 0.1 M TBAPF₆ as the supporting electrolyte.

S5. Binding Studies

¹H NMR Spectral Titration Plot

The receptor solutions of **nabp-Me₂²⁺•2PF₆⁻** (0.83 mM, CD_3CN , 298 K) were titrated by adding known quantities of a concentrated solution of TBAF, TBACl, TBABr TBAI. The anion solutions used to effect the titration contained the receptors at the same concentration as the receptor solutions into which they were being titrated so as to obviate the need to account for dilution effects during the titrations. TBACl, TBABr TBAI for the titrations were purchased from Alfa Aesar, Inc., and dried under vacuum oven for 12 h before being used.

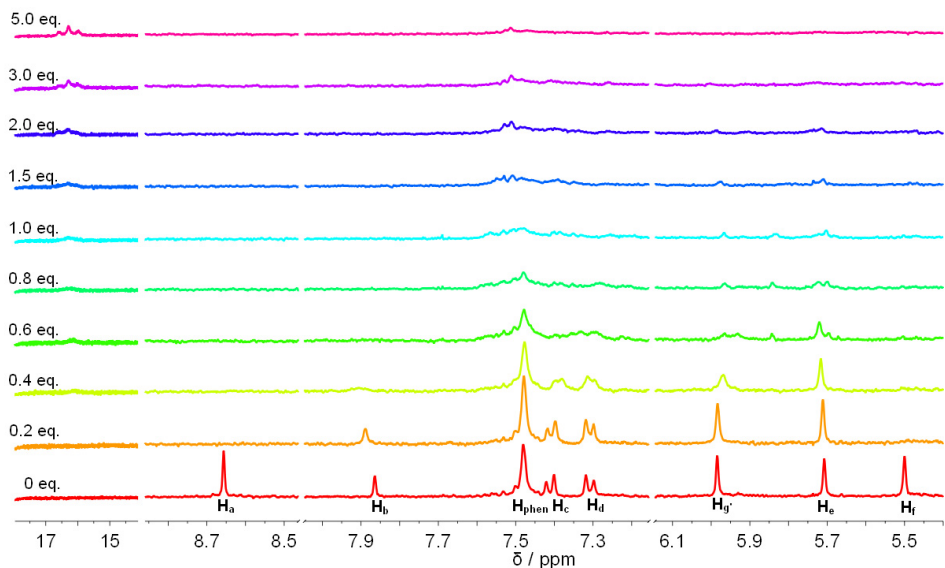


Figure S2. Macrocycle nabp-benzyl²⁺•2PF₆⁻ + n-Bu₄N•F in CD₃CN at 298 K.

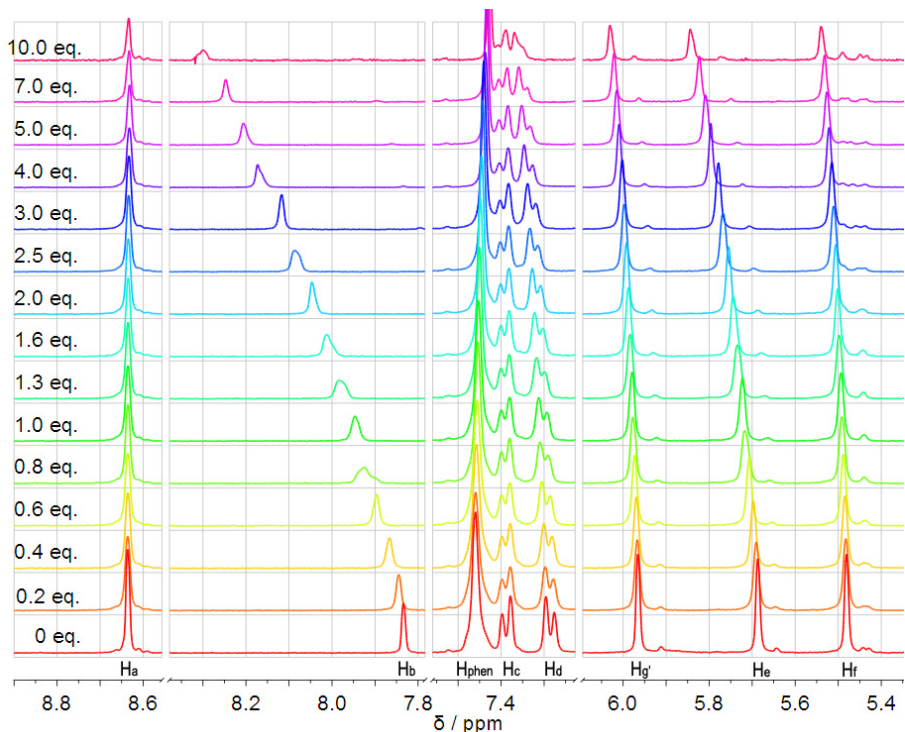


Figure S3. Macrocycle nabp-benzyl²⁺•2PF₆⁻ + n-Bu₄N•Cl in CD₃CN at 298 K.

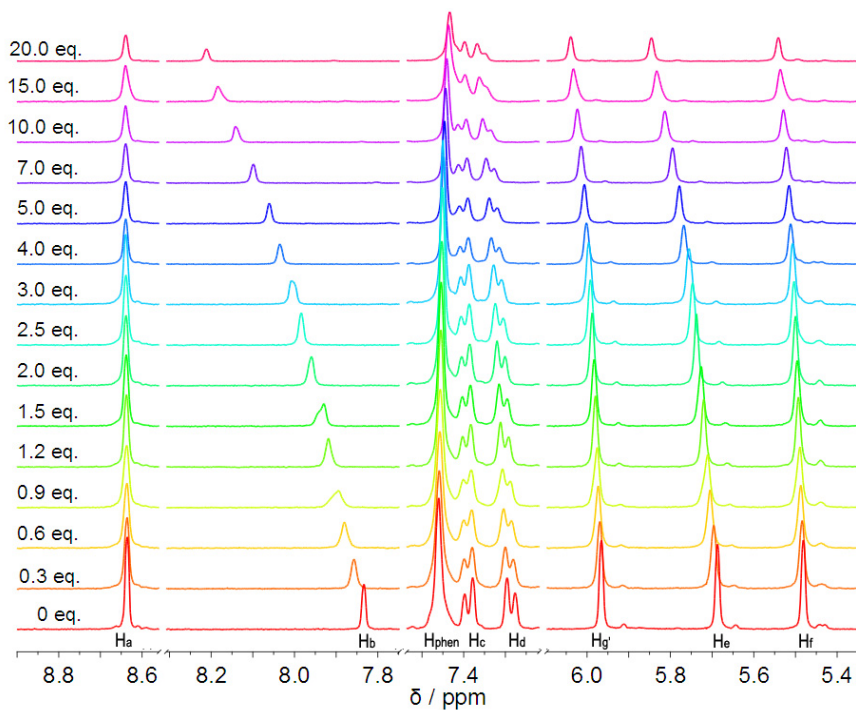


Figure S4. Macrocycle **nabp-benzyl**²⁺•2PF₆⁻ + n-Bu₄N•Br in CD₃CN at 298 K.

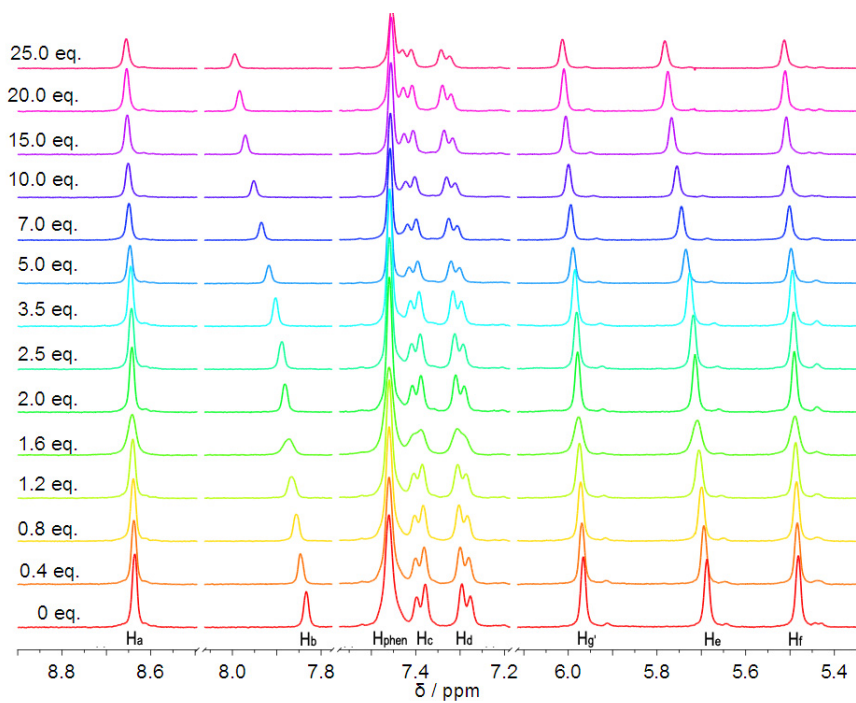


Figure S5. Macrocycle **nabp-benzyl**²⁺•2PF₆⁻ + n-Bu₄N•I in CD₃CN at 298 K.

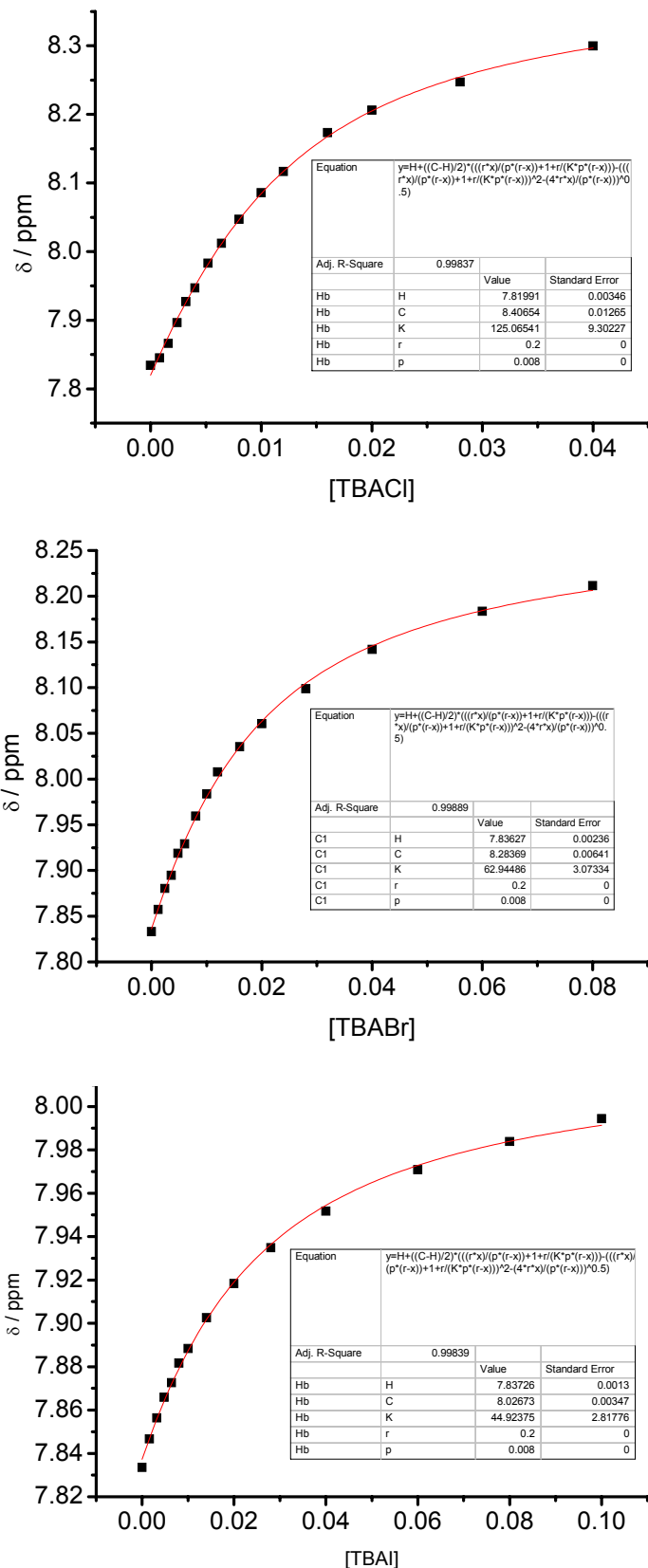


Figure S6. Fitting results of Macrocycle **nabp-benzyl²⁺•2PF₆⁻** with Cl⁻, Br⁻, I⁻ halides.

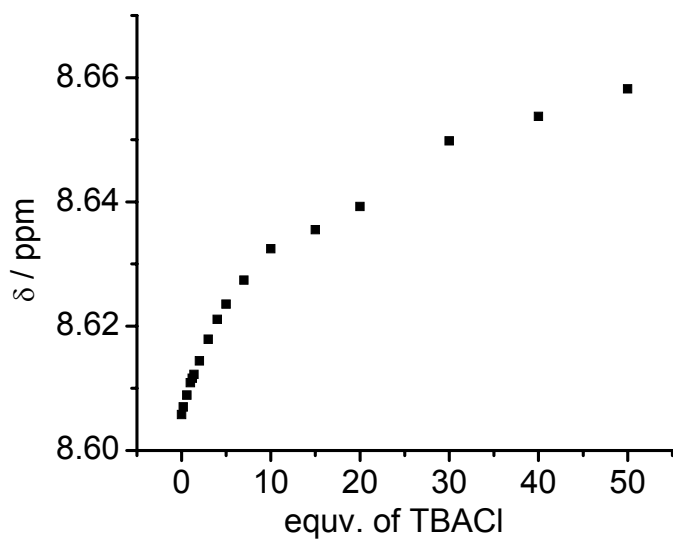
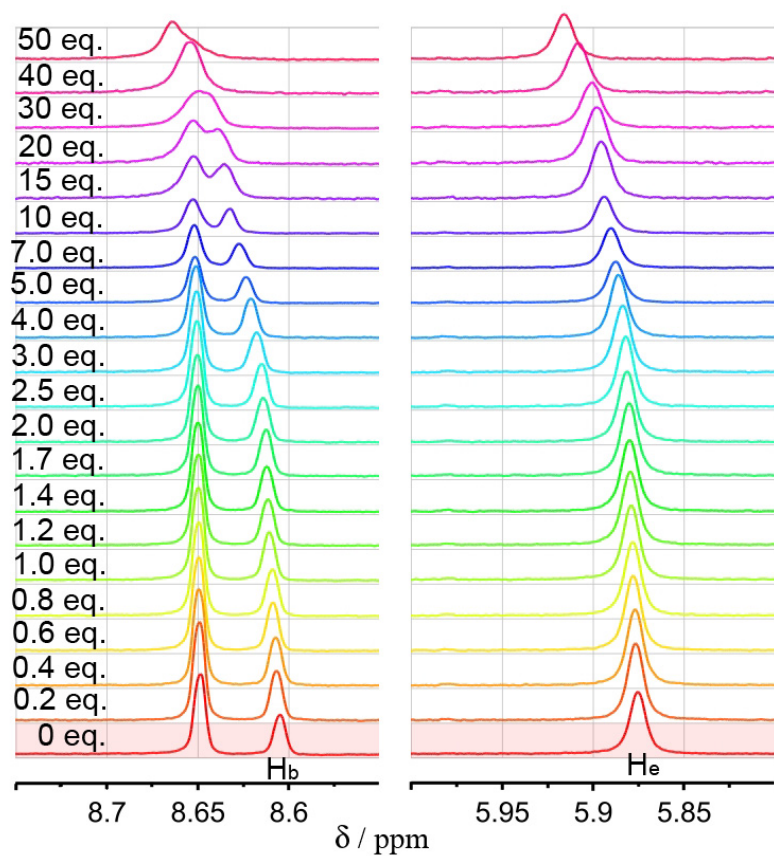


Figure S7. Macrocycle **nabp-Me₂²⁺•2PF₆⁻** + n-Bu₄N•Cl in d₆-DMSO at 298 K.

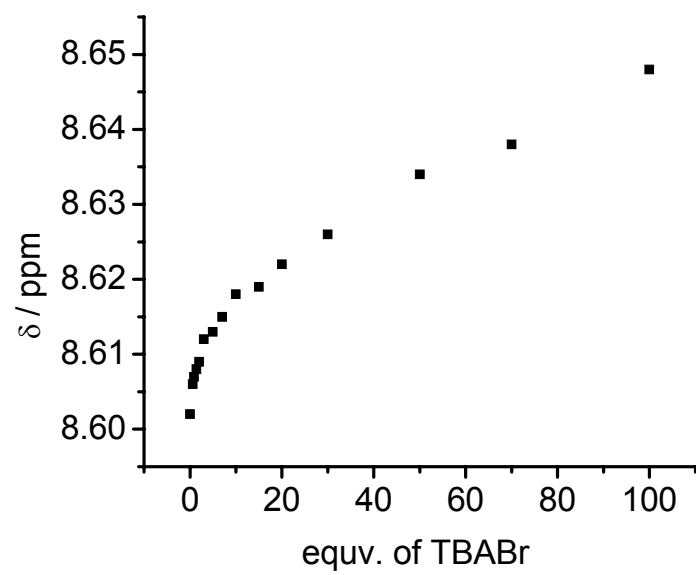
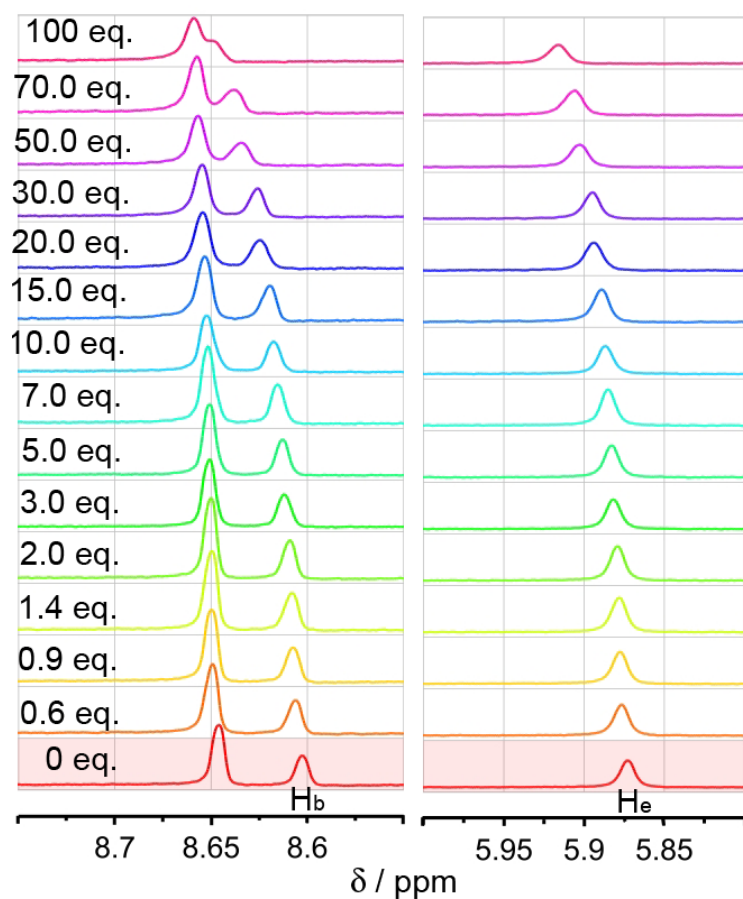


Figure S8. Macrocycle **nabp-Me₂²⁺•2PF₆⁻** + n-Bu₄N•Br in d₆-DMSO at 298 K.

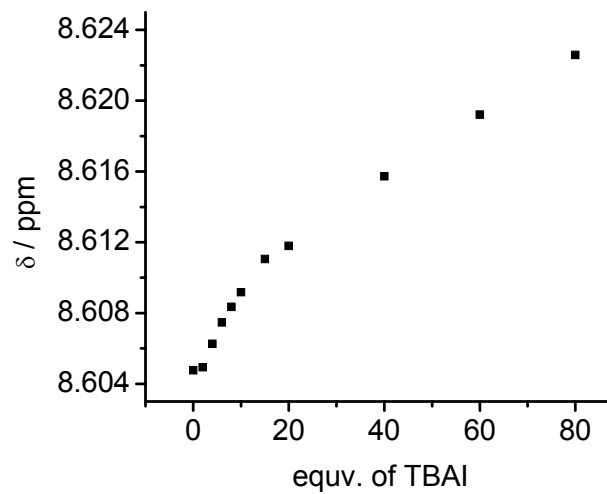
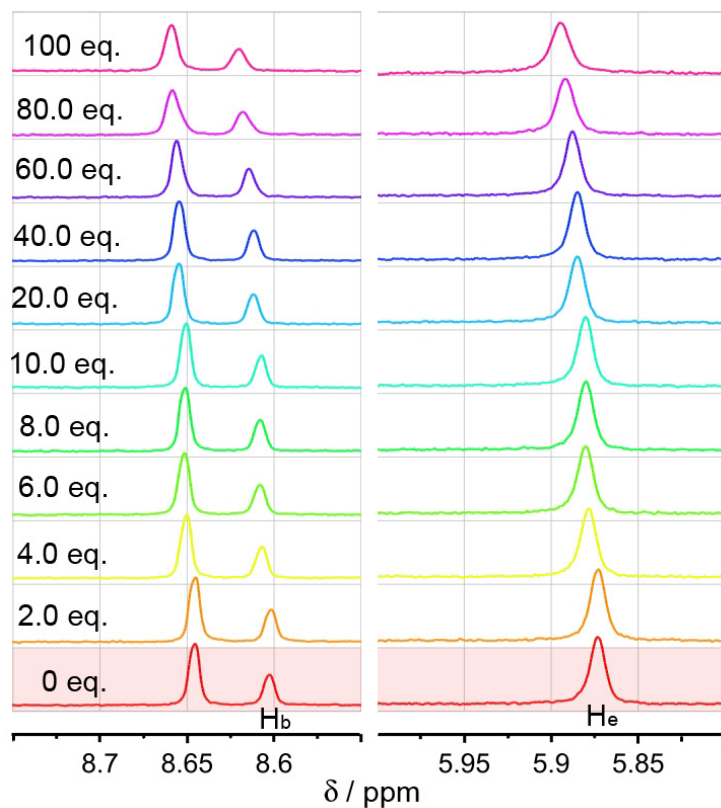


Figure S9. Macrocycle nabp-Me₂²⁺•2PF₆⁻ + n-Bu₄N•I in d₆-DMSO at 298 K.

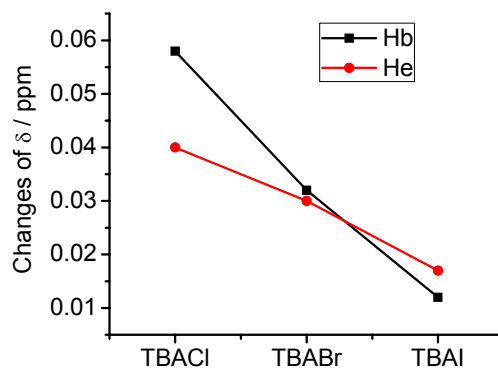


Figure S10. Chemical shifts tendency of proton H_b and H_e upon titration with Cl⁻, Br⁻ and I⁻.

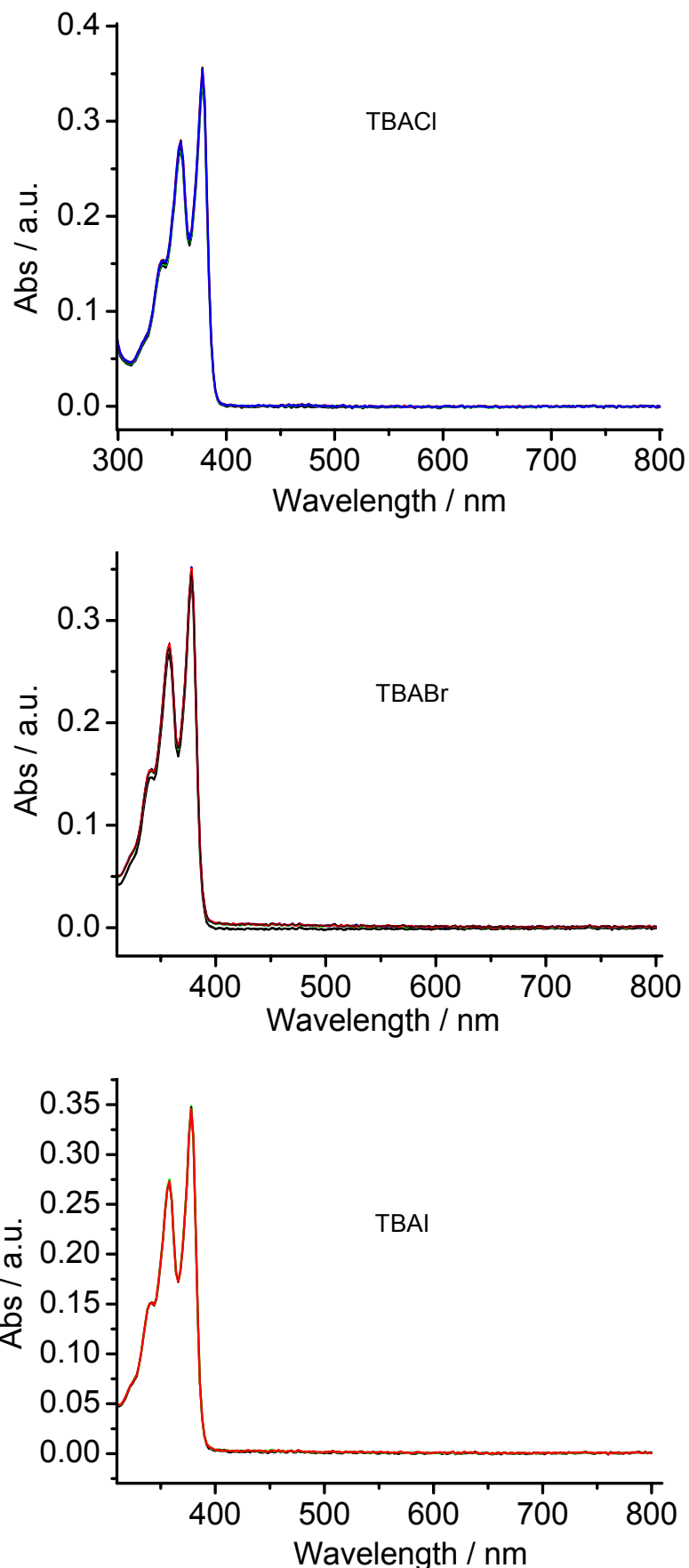


Figure S11. UV-vis-NIR spectra showing the response of **nabp-Me₂²⁺•2PF₆⁻** (1.2×10^{-5} M) upon incremental addition of Cl⁻, Br⁻, I⁻ in DMF (0-10 equivalents.).

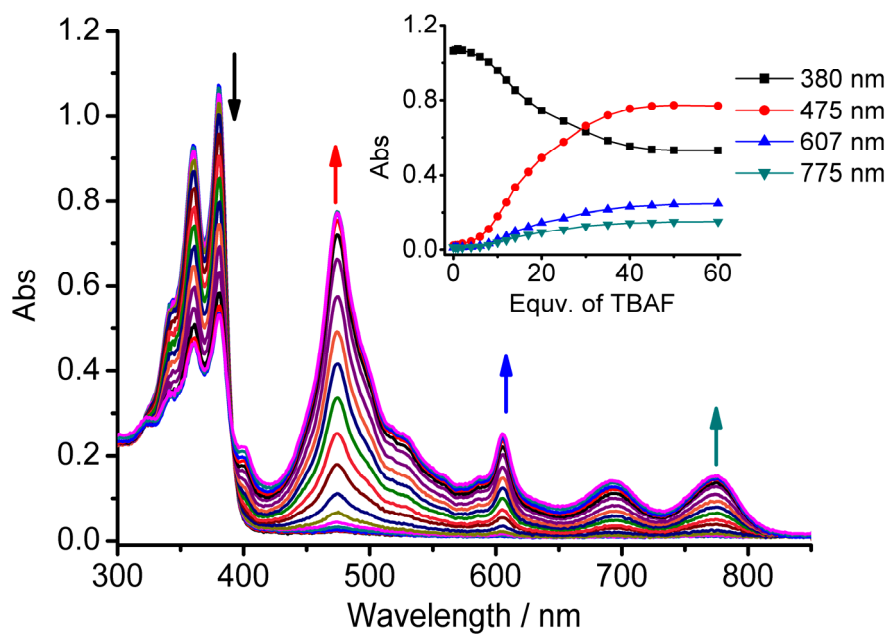


Figure S12. UV-vis-NIR spectra showing the response of **nap-Me₂²⁺•2PF₆⁻** (5.0×10^{-5} M) upon incremental addition of F⁻ in DMF.

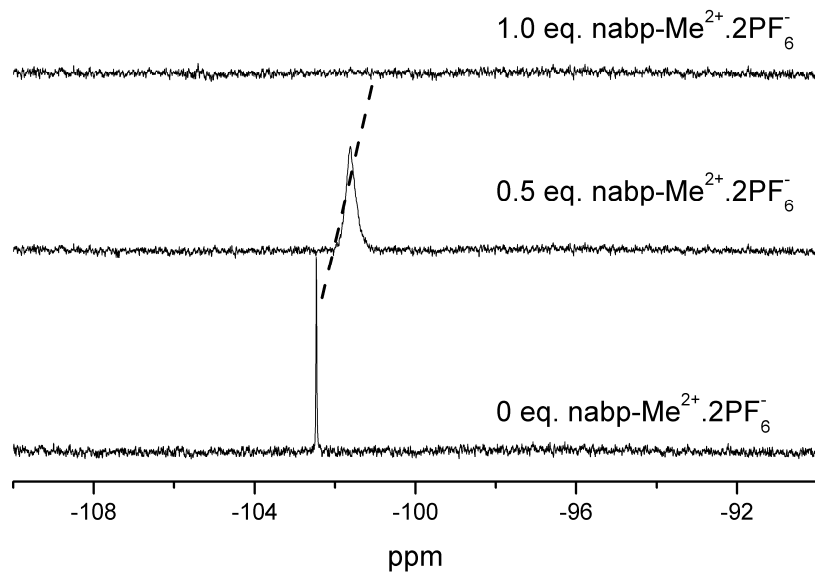


Figure S13. ¹⁹F NMR titration of F⁻ with **nap-Me₂²⁺•2PF₆⁻** showing NDI/F⁻ interaction (DMSO-*d*6, 298 K).

S6. Anion exchange experiments.

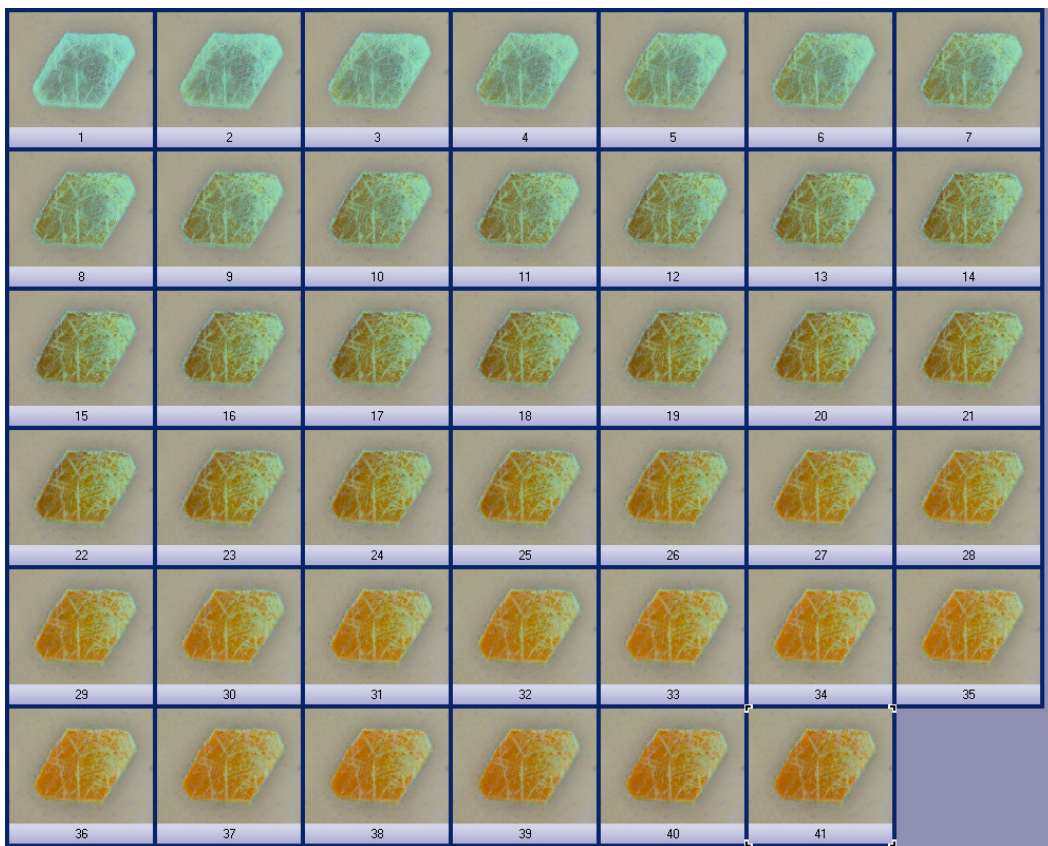


Figure S14. The *in situ* optical microscopy of **nabp-Me₂²⁺** crystals in 2 mM CH₂Cl₂ TBABr solution versus time (every 3 minutes) (scale bar: 500 μm). (there are some 1-D structure surround the crystals which were formed when the crystals in mother liquid were transferred to CH₂Cl₂ phase.).

The crystals after exchange could not be solved by single crystal X-ray diffraction due to reduction in crystallinity. Nevertheless, the crystals retain their morphology throughout, the resultant PXRD pattern after 3 days corresponds well to the pattern of the crystals before anion exchange except some peak intensity variation (Figure S13). The first peak is at a higher angle, as expected for replacement of the larger PF₆⁻ anions for the smaller halides anions. The anion exchange reaction is therefore a diffusion process occurs at the solid-liquid interface.²⁸

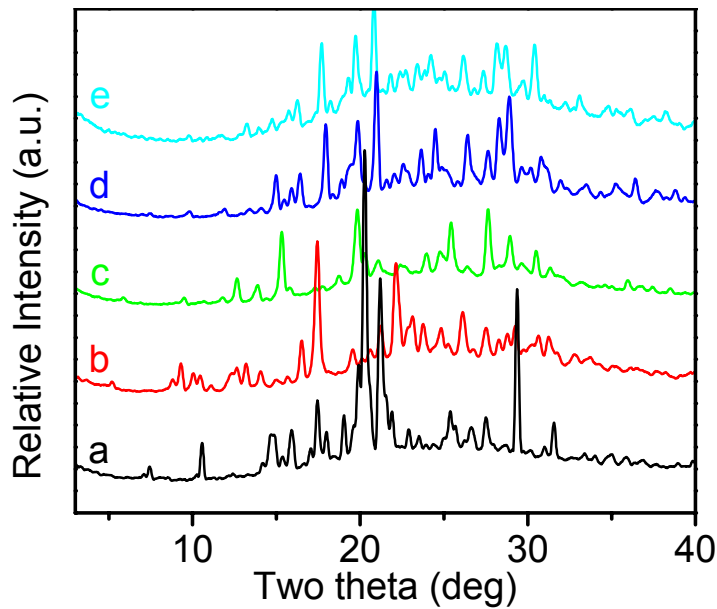


Figure S15. PXRD of **nabp-Me₂²⁺•2PF₆⁻** (a) and the solid product after 3 days exchange reaction between **nabp-Me₂²⁺•2PF₆⁻** and 0.1 M TBAF (b), TBACl (c) TBABr (d) TBAI (e).

The strong, broad IR band of the P–F group at $\sim 842\text{ cm}^{-1}$ has disappeared after immersing as-synthesized **nabp-Me₂²⁺** crystals in 0.1 M TBAF, TBACl, TBABr, TBAI solution at room temperature for 3 days (Figure S14). The cyclophane **nabp-Me₂²⁺•2PF₆⁻** exhibited stretching vibrations of the imide carbonyl groups at 1710 and 1673 cm^{-1} . In the presence of F⁻, the corresponding stretching vibration at 1710 cm^{-1} slightly shifted to 1704 cm^{-1} , the vibration at 1673 cm^{-1} shifted to 1658 cm^{-1} as a result of greater degree of single bond character in the radical anion. For chloride, weaker but similar tendency was observed. For bromide and iodide, there is no change in this region.

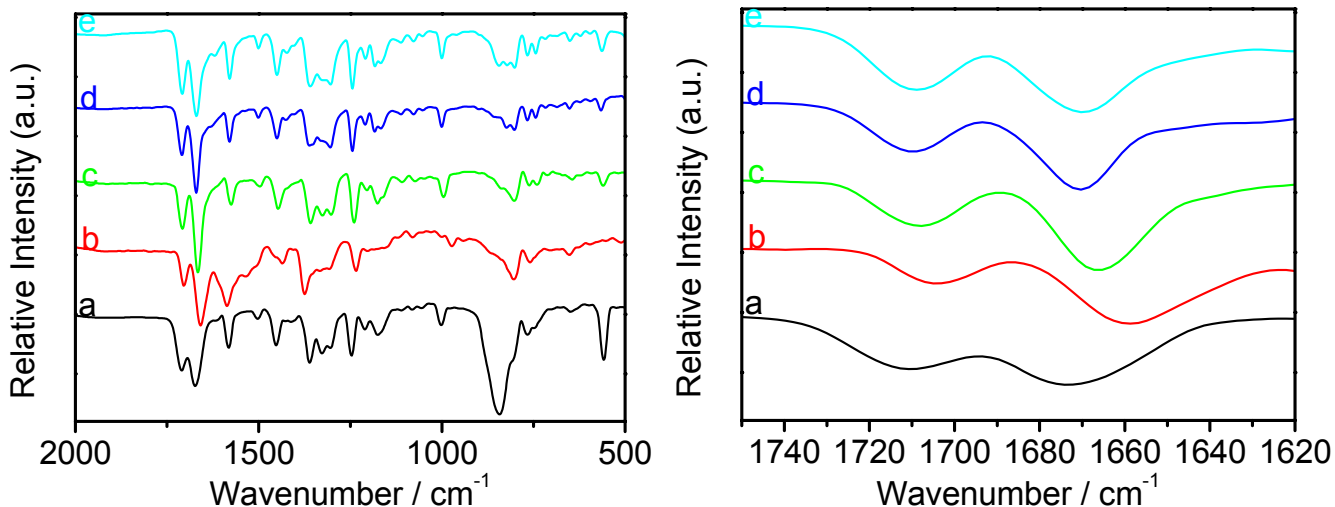


Figure S16. FTIR of **nabp-Me₂²⁺•2PF₆⁻** (a) and the solid product after 3 days exchange reaction between **nabp-Me₂²⁺•2PF₆⁻** and 0.1 M TBAF (b), TBACl, (c) TBABr, (d) TBAI (e). The magnified FT-IR spectra from 1620 to 1750 cm^{-1} were shown to show the peak shift clearly.

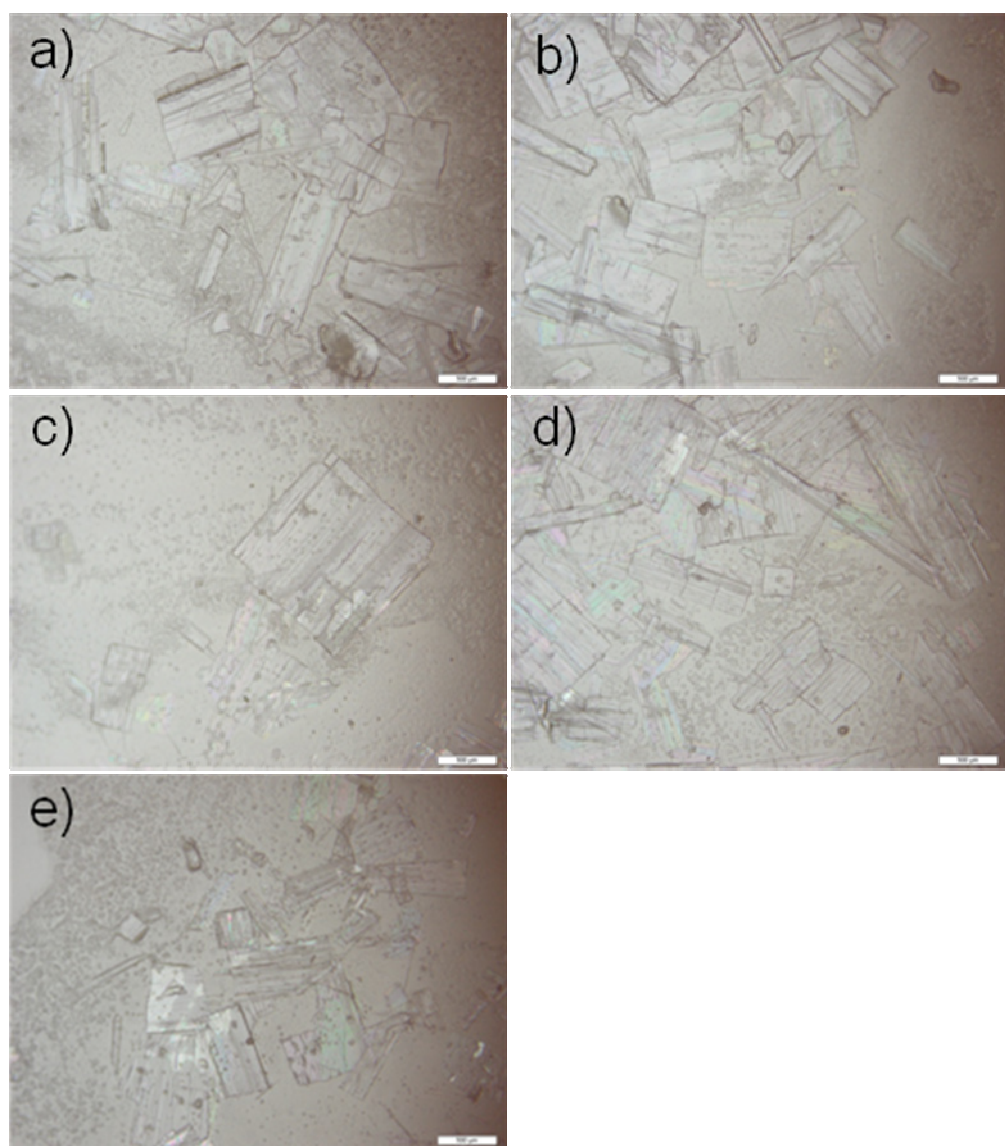


Figure S17. Optical micrographs of **nap-Me₂²⁺** crystals before (a) and after anion exchange with F⁻ (b), Cl⁻ (c), Br⁻ (d), I⁻ (e). (scale bar: 500 μm).

S7. X-ray diffraction data

Table S1. Crystallographic Information, Data Collection, and Refinement Parameters for **nabp-Me₂²⁺•2PF₆⁻**

empirical formula	C ₄₂ H ₃₇ F ₁₂ N ₁₁ O ₄ P ₂
Formula weight M_r (g·mol ⁻¹)	1049.77
temperature (K)	173(2)
crystal size (mm ³)	0.36 × 0.27 × 0.14
crystal system	Monoclinic
space group	P2(1)/c
Unit cell dimensions	$a = 13.697(2)$ Å $b = 23.188(3)$ Å $c = 14.177(2)$ Å $\alpha = 90^\circ$ $\beta = 95.173(2)^\circ$ $\gamma = 90^\circ$
V (Å ³)	4484.3(12)
Z	4
$F(000)$	2144
ρ_{calcd} (mg m ⁻³)	1.555
μ (mm ⁻¹)	0.204
θ range (deg)	2.17 to 25.00
total no. of reflns	30215
no. of independent reflns	7890 ($R_{\text{int}} = 0.0373$)
parameters	682
Final R indices [$I > 2\sigma(I)$]	$R_1 = 0.0766$, $wR_2 = 0.1910$
R indices (all data)	$R_1 = 0.0804$, $wR_2 = 0.1939$
Largest diff. peak and hole	0.805 and -0.391 e ⁻ ·Å ⁻³
goodness of fit on F^2	1.190

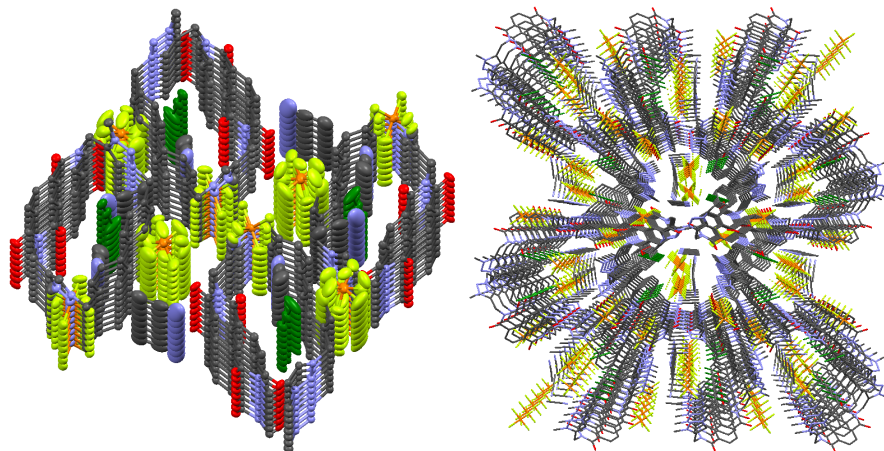


Figure S18. Channels formed by the **nabp-Me₂²⁺•2PF₆⁻** framework, running along the length of the a -axis (top) and c -axis (down) (carbon: gray; phosphate: brown; fluoride: yellow; oxygen: red; nitrogen: blue; hydrogen was omitted for clarity).

S1. J. R. Thomas, X. J. Liu, P. J. Hergenrother, *J. Am. Chem. Soc.* **2005**, *127*, 12434–12435.

S2. G. Koshkakaryan, L. M. Klivansky, D. Cao, M. Snauko, S. J. Teat, J. O. Struppe, Y. Liu, *J. Am. Chem. Soc.* **2009**, *131*, 2078–2079.